

Machine Learning-Based Modeling of the Anode Heel Effect in X-ray Beam Monte Carlo Simulations

Hussein Harb¹, Didier Benoit¹, Axel Rannou¹, Chi-Hieu Pham¹,
Valentin Tissot², Bahaa Nasr^{1,2}, and Julien Bert^{1,2*}

¹ LaTIM, University of Brest, INSERM UMR1101, Brest, France

² Brest University Hospital, France

* Author to whom any correspondence should be addressed.

E-mail: julien.bert@univ-brest.fr

Abstract. This study enhances Monte Carlo simulation accuracy in X-ray imaging by developing an AI-driven model for the anode heel effect, achieving improved beam intensity distribution and dosimetric precision. Through dynamic adjustments to beam weights on the anode and cathode sides of the X-ray tube, our machine learning model effectively replicates the asymmetry characteristic of clinical X-ray beams. Experimental results reveal dose rate increases of up to 9.6% on the cathode side and reductions of up to 12.5% on the anode side, for energy levels between 50 and 120 kVp. These experimentally optimized beam weights were integrated into the OpenGATE and GGEMS Monte Carlo toolkits, significantly advancing dosimetric simulation accuracy and the image quality which closely resembles the clinical imaging. Validation with fluence and dose actors demonstrated that the AI-based model closely mirrors clinical beam behavior, providing substantial improvements in dose consistency and accuracy over conventional X-ray models. This approach provides a robust framework for improving X-ray dosimetry, with potential applications in dose optimization, imaging quality enhancement, and radiation safety in both clinical and research settings.

Keywords: Monte Carlo Simulation, Artificial Intelligence, Anode Heel Effect, Dosimetry, Medical Imaging, Medical Physics.

1. Introduction

X-ray imaging plays a pivotal role in both diagnostic and interventional medicine. Due to its ionizing nature, optimizing imaging systems, protocols, and reconstruction methods is crucial to maintaining high image quality while minimizing patient exposure. In this context, Monte Carlo simulation remains an indispensable tool in medical physics, offering unmatched accuracy in modeling photon-matter interactions and dose deposition [1, 2]. This approach allows the simulation of the entire X-ray tube system [3], enabling the generation of highly realistic photon spectra and spatial distributions. Nevertheless, Monte Carlo simulations are computationally intensive.

A common approach to reduce computational costs is to divide the simulation into two phases: (1) a simulation of the X-ray tube alone, generating a phase space file, and (2) a patient-dependent phase where this file is reused, eliminating the need for repeated

tube simulations. However, for simulations that require a large number of particles and extensive statistics, the phase space file can reach hundreds of gigabytes, making the simulation impractical. Generally, a virtual source is preferred. This refers to an analytical mathematical model that represents the distribution and correlation of particles in the phase space [4]. Such model requires only few parameters saving stored memory and can rapidly produce particle distributions on demand. The main drawback is that such models are often an approximation and only represents the predominant characteristics of the source.

For example, the anode heel effect of the X-ray tube is rarely considered. This affect the beam intensity asymmetry arising from the angled geometry of the X-ray tube anode. This effect causes X-rays directed toward the cathode side to exhibit higher intensities, while those toward the anode side are attenuated due to self-absorption within the anode [5, 6]. This asymmetry impacts both dose distribution and image quality, particularly in wide-field imaging applications [7]. Neglecting the anode heel effect in MC simulations can lead to significant discrepancies between simulated and real measurements [8].

Recent studies have explored various approaches to model the anode heel effect, including empirical adjustments and analytical formulations [9]. However, these methods often lack flexibility or fail to account for energy-dependent variations in beam intensity. Advances in artificial intelligence (AI) present a promising solution for capturing complex, non-linear phenomena like the anode heel effect. Machine learning models, trained on experimental data, can generalize across a wide range of energy levels and beam geometries, offering a scalable alternative to traditional methods [10].

In this study, we propose an AI-driven approach to accurately model the anode heel effect and integrate it into MC simulations. By combining experimental measurements with a Gradient Boosting Regression model, we predict beam intensity distributions across energy levels ranging from 50 to 120 kVp. These predictions are seamlessly incorporated into the OpenGATE [2] and GGEMS [11] MC toolkits, enabling precise simulation in both research and clinical settings. Our approach not only addresses a critical gap in X-ray beam modeling but also lays the groundwork for future advancements in radiation safety and imaging optimization.

2. Materials and Methods

In this study, we modeled a virtual source that replicate the characteristics and behavior of a real X-ray tube. This tube consists of a cathode that emits electrons through thermionic emission and a tungsten anode where these electrons are accelerated under high voltage and converted into X-ray photons via bremsstrahlung and characteristic interactions [12,13]. Tube voltages ranging from 50 to 120 kVp were employed to simulate various clinical imaging scenarios. The anode's angled geometry plays a critical role in producing the non-uniform intensity distribution of the beam, contributing to the anode heel effect.

2.1. Standard X-ray tube virtual source model

A virtual source model consists of mathematically modeling the emission of photons from the tube. In Monte Carlo simulations, for each randomly emitted particle, the parameters of the photon have to be determined. Each photon $\gamma(E, \mathbf{p}, \mathbf{d})$, is defined by its energy E , its position $\mathbf{p} = \{p_x, p_y, p_z\}^T$, and its momentum (direction) $\mathbf{d} = \{d_x, d_y, d_z\}^T$. The position \mathbf{p} is defined by the emission area on the anode, which corresponds to a rectangular surface measured in millimeters (mm). For each new particle, this position is determined randomly and uniformly over this surface, $\mathbf{p} \sim \mathcal{U}(S)$, where \mathcal{U} represents the uniform distribution, and S denotes the surface.

The particle's momentum is defined by the Euler angles (α : *altitude*, β : *azimuthal*) of the particle emission. In the standard model particles are emitted following an angular uniform distribution. In this case the random sampling should not be done over the altitude angle α , but rather over its cosine $\cos(\alpha)$. This can be expressed as:

$$\frac{d\Omega}{d \cos \alpha} = 1 \quad (1)$$

where $d\Omega$ is the differential solid angle and $\cos(\alpha)$ is the cosine of the polar angle α . Therefore, the momentum direction \mathbf{d} is sampled randomly with a probability distribution proportional to $\mathcal{U}(\cos \alpha)$. The azimuthal angle β is also sampled randomly and uniformly between 0 and 2π : $\beta \sim \mathcal{U}(0, 2\pi)$. However, the angle of the beam's aperture \mathcal{A} must also be taken into account. The angle α is then obtained as follows:

$$\alpha = \cos^{-1}(1 + \xi \cdot [\cos(\mathcal{A}) - 1]) \quad (2)$$

where ξ is a uniform random number between $[0, 1)$. Based on the two angles α and β , the direction of the particle \mathbf{d} can be defined as follows:

$$\mathbf{d} = \begin{bmatrix} \cos \beta \cdot \sin \alpha \\ \sin \beta \cdot \sin \alpha \\ \cos \alpha \end{bmatrix} \quad (3)$$

Most of the time, the tube is also oriented around the patient, then a transformation including rotation and translation must be applied to the particle:

$$\begin{cases} \mathbf{p}' = \mathbf{T}_{xyz}\mathbf{p} \\ \mathbf{d}' = \mathbf{R}_{\psi\theta\phi}\mathbf{d} \end{cases} \quad (4)$$

where \mathbf{p}' is the final particle emitting position, \mathbf{d}' is the final particle momentum, \mathbf{R} and \mathbf{T} are the rotation and translation matrices of the X-ray tube respectively. Collimation can also be applied, whether to achieve a fan beam in diagnostic CT or to reduce the field of view in fluoroscopy.

Two strategies are commonly used. The first involves defining the collimator as a patient-dependent component, as it can be tailored to the specific clinical case. In this strategy, the collimator is simulated each time using Monte Carlo methods, which also allows for the calculation of beam scattering (penumbra). This approach is particularly useful when filters, such as wedges or bowtie filters, are present within the beam. If the

collimation is fixed and no filters are used, a second strategy involves employing a ray-tracing method within the virtual source model. Essentially, the particle path is checked to determine if it hits the collimator. If it does, a new particle is emitted. This process is repeated until a particle successfully exits the source, similar to a rejection sampling method.

Regarding the determination of the particle's energy, a realistic emission spectrum is used. Existing model, such as the TASMIP model [14] or, more recently, CASIM [15], which is the default model in the Python library SpekPy [9], can be used to provide spectrum histogram $f(E_i)$ based on the tube parameters, such as voltage, anode material, or filtration layers. The particle energy is then randomly sampled by using the cumulative distribution function (CDF) obtained by normalizing the histogram ($\sum f(E_i) = 1$), and by cumulating the bin value as follow:

$$F(E_k) = \sum_{i=1}^k f_{\text{norm}}(E_i) \quad (5)$$

where $F(E_k)$ represents the cumulative probability up to the bin k . Given a random number $\xi \sim \mathcal{U}(0, 1)$, the energy E_ξ is determined by finding the smallest bin index k where:

$$F(E_k) \leq \xi < F(E_{k+1}) \quad (6)$$

Since the real spectrum is continuous rather than discrete, the final particle energy is determined using linear interpolation.

2.2. Incorporating the Anode Heel Effect

The anode heel effect introduces significant variations in beam intensity according to the particle emitted angle. To accurately model these variations, we introduce weighting factors in the random angle selection. These weights $\mathcal{W}(\alpha, \beta, E)$ depends of the angle but also on the energy. The naive way consist of storing every weight into a multidimensional histogram for every possible parameters. Each value \mathcal{W}_i can be defined from simulation or experimentally by comparing the density probability of emission from image intensity or measures doses. Similarly to the random energy definition, the weights are transform into cumulative distribution function (CDF) for each energy bin.

The strategy consists to random the particle energy E according to the spectrum, and then select the corresponding CDF for $\mathcal{W}(\alpha, \beta)$ to also randomly select a angle couple (α, β) . A linear interpolation is applied of the angle calculation in order to smooth the sampling effect between value inside histograms. The last step consist, as the standard model, to convert the particle's emission angle into particle's momentum and consider the x-ray tube position and orientation.

2.3. Modeling the Weights with Machine Learning

To achieve a realistic simulation and cover all parameters, it is necessary to determine a significant number of weights, which can be complicated and tedious. When the relationship between parameters is not overly complex and the values are continuous,

a mathematical model is often used. The strategy involves fitting a model to the data to determine the coefficients that describe it. This reduces the amount of data needed to store and describe the virtual source.

However, most of the time, the correlations between parameters are significant, making it difficult to derive a model, especially with complex sources such as those in radiotherapy [16]. The ability of AI to learn a complex model with few coefficients has been explored, particularly for source models in external radiotherapy calculated by Monte Carlo simulation [4]. In this study, we propose using AI for its ability to interpolate complex models. That is, to capture the complexity of the weights \mathcal{W} as a function of various parameters using only a few values to construct it. The aim is to reduce the number of experimental measurements or simulations to build the model.

2.3.1. Implementation In the pre-implemented source in OpenGATE [2], the function `source.direction.type = 'iso'` was used to generate an isotropic, uniform source with no variation in the weights. To integrate our model into the Monte Carlo (MC) toolkits OpenGATE and GGEMS [11], an existing function—configured with `source.direction.type = "histogram"`—was utilized to assign the predicted weights. This configuration is similar to 'iso', but it allows the emission of primary particles with directional distributions weighted by custom-defined histograms for θ and ϕ angles. The weights are specified using `source.direction.histogram_phi_weights` at each energy level and for each angle defined via `source.direction.histogram_phi_angles`.

The ϕ angles were calculated using the following equation:

$$\phi = \arctan\left(\frac{d}{70\text{cm}}\right) \quad (7)$$

where d is the distance from the center (reference) to the dose reading point.

In addition, to transition between points along the anode-cathode axis, linear interpolation was applied to the weights. These weights were adjusted for the tube potentials used, thereby accounting for the energy-dependent nature of the anode heel effect. For energies not explicitly defined in these increments, the predicted weights from the trained GBR model were employed.

2.4. Evaluation study

2.4.1. Experimental Setup for Data Collection For a better modeling of the system used in our clinical application, and show the capability of machine learning interpolation, we decide to determine the weights \mathcal{W} by using experimental measurements. The considered system in our study was the Cios Alpha X-ray machine (Siemens Healthcare Headquarters, 91052 Erlangen, Germany) [17]. Dose rate measurements were conducted along the anode-cathode axis using a PTW-NOMEX Multimeter dosimeter with measuring error less than 5% [18]. To ensure measurement consistency, the dosimeter was placed at predefined positions along the anode-cathode axis, maintaining a fixed source-to-detector distance at 70 cm, as shown in **Figure 1**. Measurements were performed for tube potentials ranging from 50 to 120 kVp with a 10 kVp step. To account for variations in exposure conditions, dose rates were normalized relative to the intensity of the central beam.

We conducted a total of 25 measurements per energy level, beginning with the central reference measurement at the intersection of the laser cross "Beam Center". From there, we incrementally shifted by 1 cm in both directions, recording dose rates until we reached 9 cm, which marked the edge of the X-ray beam coverage on both sides. To confirm this boundary, we took an additional measurement at 10 cm. Further measurements were performed at 15 cm and 20 cm on both sides to ensure the absence of beam leakage that could impact the accuracy of the results.

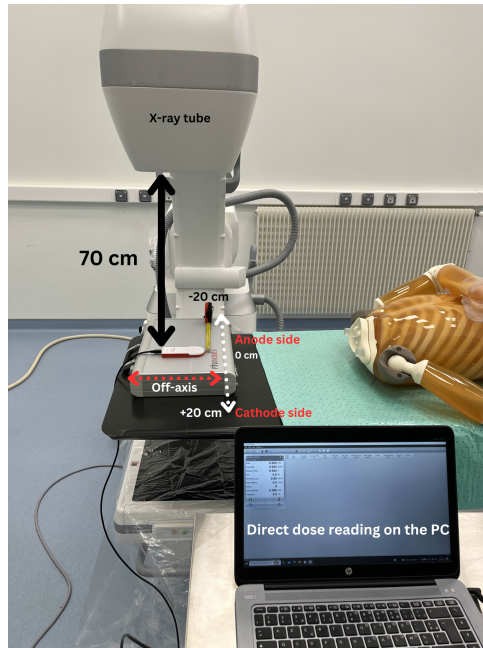


Figure 1. Experimental setup for measuring dose rates along the anode-cathode axis using the PTW-NOMEX Multimeter dosimeter.

2.4.2. Machine Learning Model Parameterization The collected dose rates were used to calculate relative weights along the anode-cathode axis. These weights represent the ratio of the measured dose rate at a given position to the central beam intensity as explained in the following equation:

$$W(x) = \frac{I(x)}{I_0} \quad (8)$$

where I_0 is the central beam intensity, and $I(x)$ is the experimentally derived weight at distance x .

The training dataset includes these weights from experimental measurements but also tube voltage (kVp) and distance from the beam center in (cm). The data were split into training (80%) and testing (20%) subsets, ensuring proper validation.

A total of six machine learning algorithms were evaluated, including Linear Regression [19], Support Vector Regression (SVR) [20], and Gradient Boosting Regressor (GBR) [21]. The GBR was chosen for its superior ability to capture the non-linear relationships among tube potential, beam position, and intensity. The models underwent fine-tuning via hyperparameter optimization with 5-fold cross-validation to minimize

overfitting and enhance accuracy. During optimization, the learning rate was varied between 0.001 and 0.1, while the number of estimators ranged from 100 to 1000. The features—'DoseRate', 'Energy', and 'Theta'—served as the input variables (X), and 'Weight' was used as the target variable (Y) for training and testing.

Model performance was assessed using the Mean Squared Error (MSE) and the coefficient of determination R^2 , with the GBR achieving the best results.

$$\text{MSE} = \frac{1}{n} \sum_{i=1}^n (y_i - \hat{y}_i)^2, \quad (9)$$

where y_i represents the actual beam weight at a given position and energy, and \hat{y}_i is the model-predicted value.

$$R^2 = 1 - \frac{\sum_{i=1}^n (y_i - \hat{y}_i)^2}{\sum_{i=1}^n (y_i - \bar{y})^2}, \quad (10)$$

where \bar{y} is the mean of the observed values. A high R^2 score reflects the model's efficacy in accurately predicting beam weights across varying tube potentials and spatial positions.

2.4.3. Fluence evaluation Two validation tests were conducted to assess how the anode heel effect influences radiation distribution.

In the first test, 20 virtual detectors were evenly positioned along the anode-cathode axis to measure radiation intensity using 10^9 simulated photons. These detectors recorded fluence levels both with and without AI-predicted anode heel effect adjustments. The results demonstrated an asymmetrical radiation distribution, aligning with experimental observations and confirming the AI model's ability to replicate the effect.

In the second test, a single detector was placed 50 cm from the X-ray source to evaluate dose distribution. The resulting dose maps, generated with and without accounting for the anode heel effect, exhibited significant differences in intensity patterns. This further validated the AI model's accuracy in capturing the phenomenon.

2.4.4. Impact on image quality An anthropomorphic phantom, PH-2E—a modified version of PBU-60 [22] with pathologies—was used to simulate a patient scenario in both the experimental setup and the Monte Carlo simulation, as shown in **Figure 8**. The phantom represents a human with a height of 165 cm and a weight of 60 kg. An anterior-posterior (AP) X-ray of the upper chest was performed at 75 kVp using the Cios Alpha X-ray machine at PLATIMED. The same parameters were applied in the Monte Carlo simulation, first using an isotropic uniform X-ray beam distribution and then incorporating the anode heel effect into the beam. Finally, the percentage relative errors were calculated to evaluate the impact of the anode heel effect in producing a real-world modulated X-ray beam.

3. Results

3.1. Modeling Results

Figure 2 presents the angular distribution of photons obtained from the two models described in Section 2, using a total of 5×10^6 samples. The left panel illustrates the uniform angular distribution in solid angle, where the emission angles (α, β) are sampled uniformly. The color scale, transitioning from light to dark blue, represents the number of sampled photons. This model assumes an idealized X-ray source with no directional intensity variations, serving as a baseline for comparison. In contrast, the right panel incorporates the anode heel effect, where self-absorption within the anode leads to greater attenuation of lower-energy photons on the anode side. This results in an asymmetric distribution, with reduced intensity on the left (anode) and increased photon emission on the right (cathode). The accompanying color scale quantifies the number of samples per angular bin, highlighting the directional intensity variation introduced by the anode heel effect. This model provides a more realistic representation of X-ray tube emissions, influencing radiation dose calculations and image quality in medical imaging applications.

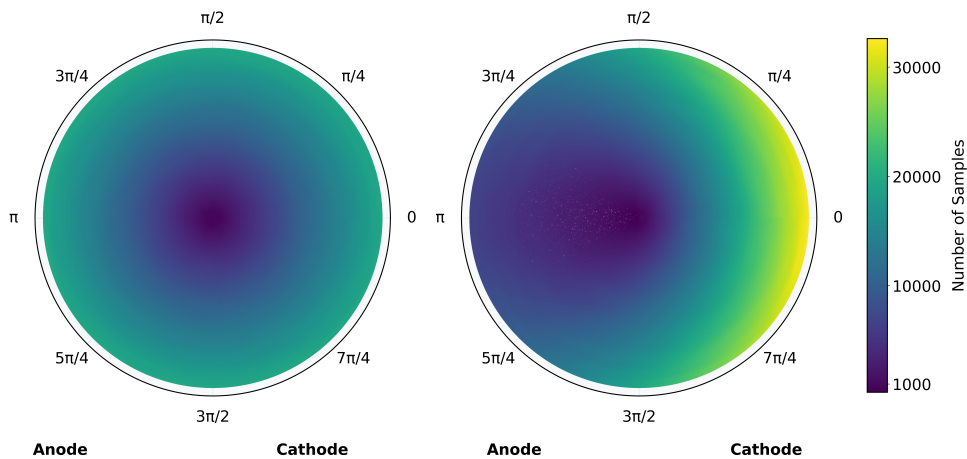


Figure 2. Comparison of X-ray beam angular distributions. Left: A uniform emission model without the anode heel effect, where photon intensities are evenly distributed. Right: A model incorporating the anode heel effect, showing reduced intensity on the anode side due to self-absorption within the anode.

3.2. Experimental Results

Dose rate measurements conducted for tube potentials ranging from 50 to 120 kVp demonstrated clear asymmetry in intensity along the anode-cathode axis. As shown in **Figure 3**, the dose rates increased by approximately 8.8% to 9.6% on the cathode side and decreased by up to 12.5% on the anode side at distances of 5–9 cm. This gradient was more pronounced at higher tube potentials, underscoring the energy-dependent nature of the anode heel effect.

Relative intensity weights, derived from these measurements, were normalized to the central beam intensity. The resulting weight distribution, shown in **Figure 4** and the

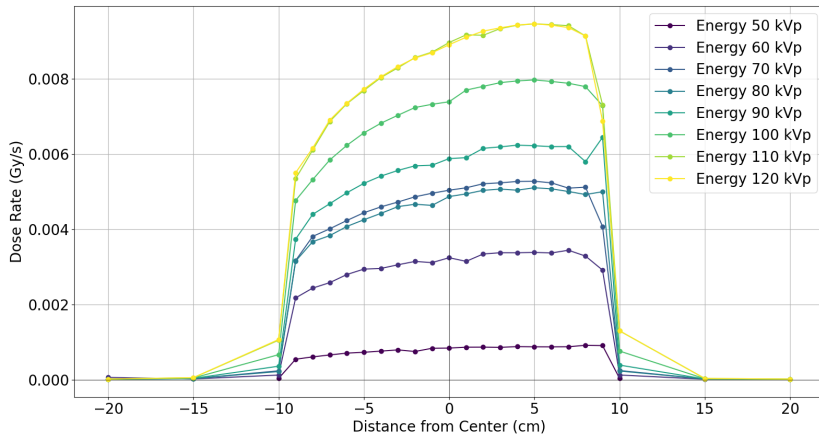


Figure 3. Dose rate plots for different energy levels between 50 kVp and 120 kVp (in steps of 10 kVp) as a function of the distance from the center of the X-ray beam (cm), with the negative side representing the anode and the positive side representing the cathode.

weight differences relative to the beam center (reference value of 1) depicted in **Figure 5**, confirmed a consistent asymmetry, with higher weights on the cathode side and lower weights on the anode side. These weights were further used to parameterize the AI model.

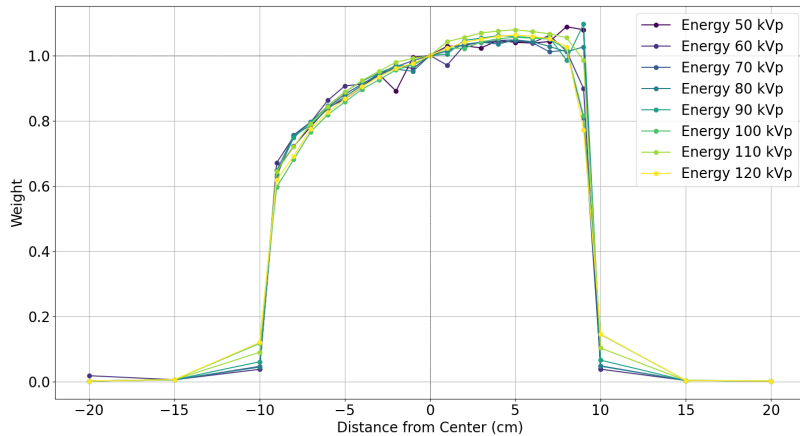


Figure 4. Weight distributions for energy levels between 50 kVp and 120 kVp (in 10 kVp steps) plotted against the distance from the X-ray beam center (cm), with the anode positioned on the negative side and the cathode on the positive side.

3.3. AI Model Training and Performance

The Gradient Boosting Regressor (GBR) model exhibited superior performance in predicting the non-linear intensity variations associated with the anode heel effect. Model evaluation metrics, summarized in **Table 1**, revealed a Mean Squared Error (MSE) of 0.0019 and a coefficient of determination R^2 of 0.9631, indicating high predictive accuracy.

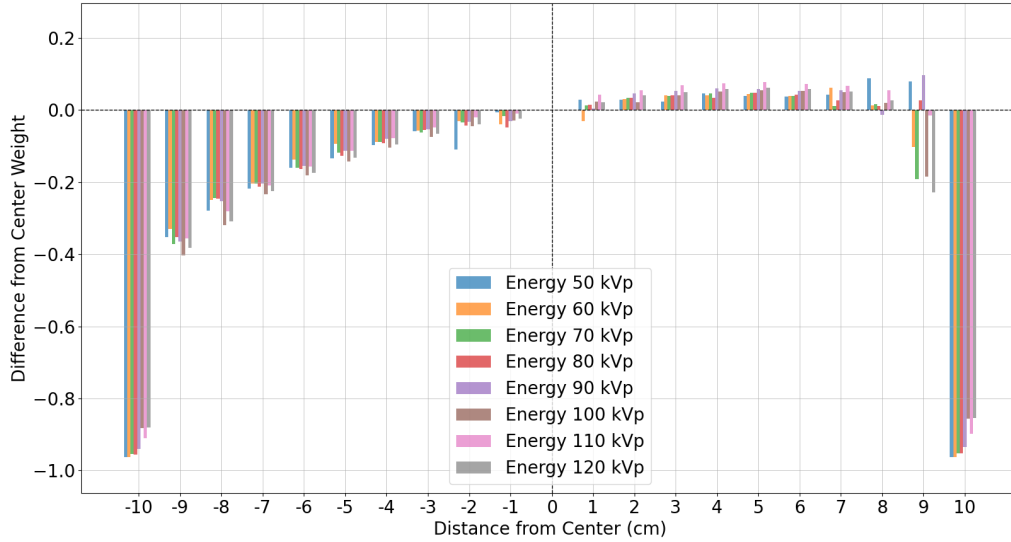


Figure 5. Weight Difference Bar Plots Across Different Distances and Energies

Table 1. Evaluation of Different Machine Learning Models in Order of Performance

Model	Mean Cross-Validation MSE	Test MSE	Test R^2
LinearRegression	0.0333	0.0432	0.7909
MLPRegressor	0.0118	0.0200	0.9030
SVR	0.0102	0.0174	0.9159
RandomForestRegressor	0.0039	0.0024	0.9284
DecisionTreeRegressor	0.0042	0.0015	0.9429
GradientBoostingRegressor	0.0019	0.0014	0.9631

3.4. Validation in Monte Carlo Simulations

3.4.1. Fluence Comparison Fluence measurements conducted using 20 actors positioned along the anode-cathode axis confirmed the AI model's ability to replicate the anode heel effect. As shown in **Figure 6**, the fluence distribution exhibited higher intensities on the cathode side and lower intensities on the anode side when the AI-predicted weights were applied. In contrast, simulations without the anode heel effect showed a uniform fluence distribution, lacking the characteristic asymmetry.

3.4.2. Dose Map Analysis Dose map validation was conducted using a single actor positioned 50 cm from the source. As shown in **Figure 7**, significant differences in intensity distribution were observed between simulations with (left) and without (right) the anode heel effect. The AI-predicted weights successfully reproduced the observed asymmetry, validating the model's integration into the Monte Carlo framework.

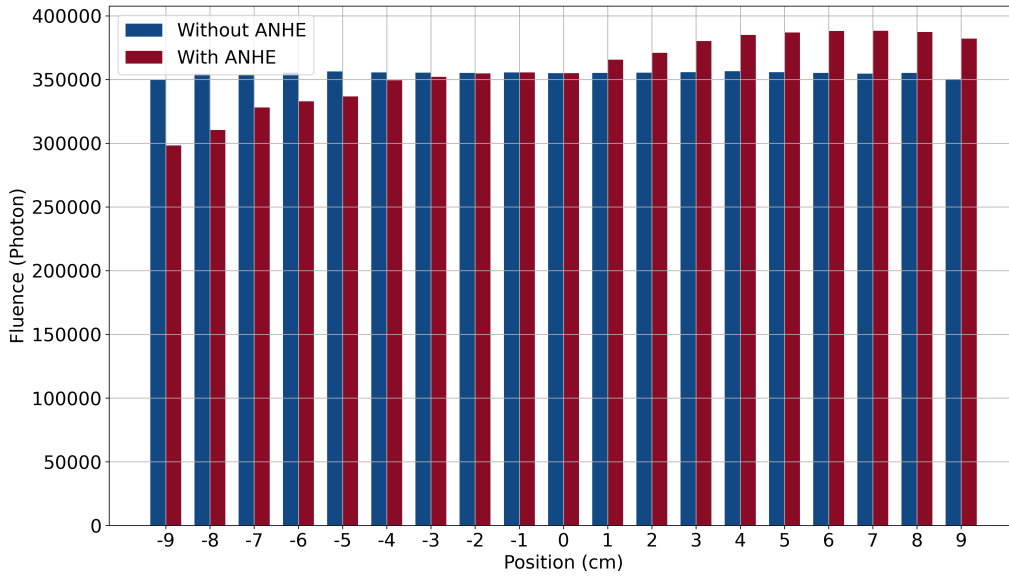


Figure 6. Fluence comparison along the anode-cathode axis (negative to positive position values). The AI-enhanced model (red) with anode heel effect (ANHE) correctly reproduces the asymmetry introduced by the anode heel effect, whereas the standard isotropic model (blue) exhibits uniform fluence distribution.

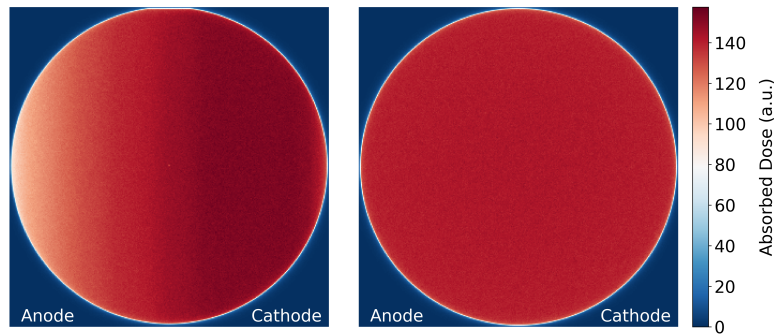


Figure 7. Dose Map Validation: Anode Heel Effect vs. Uniform Emission

3.4.3. Phantom Dose Assessment **Figure 8** shows the comparison of the experimental X-ray image with two simulated models: ISO (isotropic) and ANHE (Anode Heel Effect). Using the same parameters and 10^9 photons, the ANHE simulation closely resembles the experimental image, while the ISO model appears more blurred. Relative difference maps indicate that the ISO model underestimates certain structures, whereas the ANHE model improves accuracy. The ANHE-ISO difference highlights significant regional variations, particularly in the lungs. Overall, the ANHE model provides a more realistic approximation, emphasizing the importance of incorporating anode heel effect in simulations.

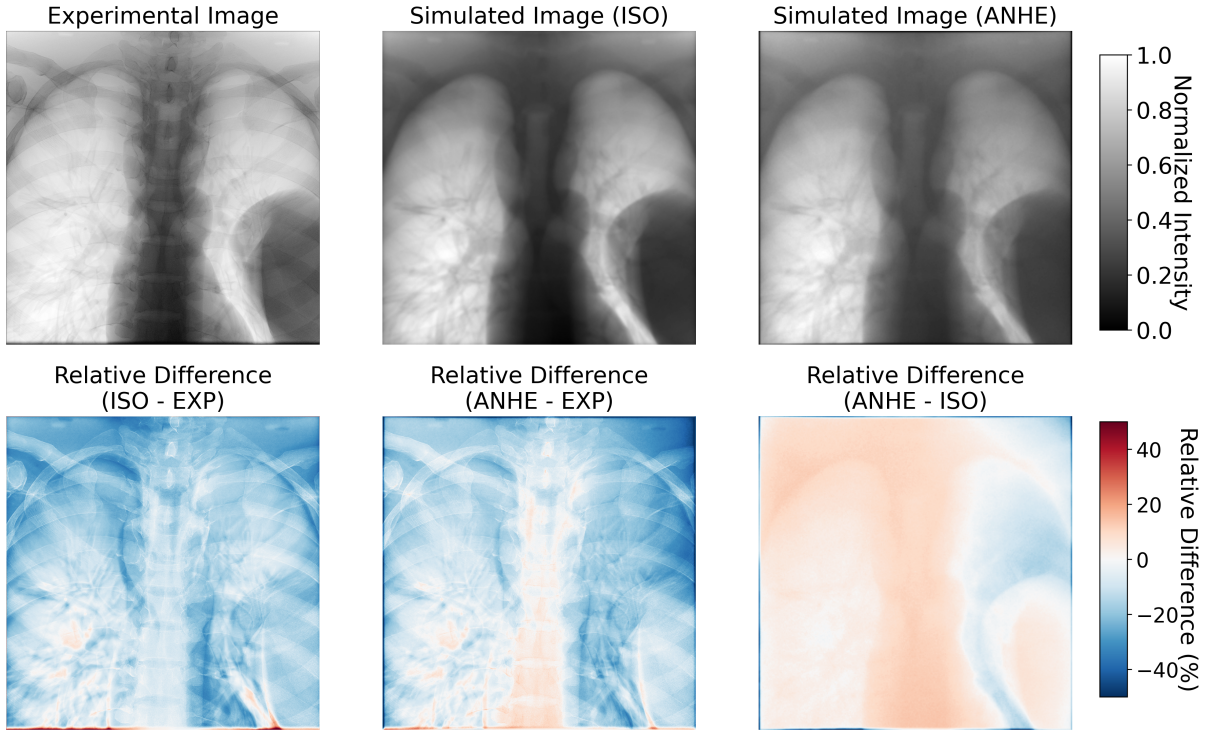


Figure 8. The first row shows X-ray images of the same phantom. From left to right: the experimental (EXP) image, the simulated image using an isotropic (ISO) source, and the simulated image using the anode heel effect (ANHE) modeled source, all in grayscale. The second row presents the relative percentage difference. From left to right: the difference between the EXP and ISO images, the difference between the EXP and ANHE images, and the difference between the ISO and ANHE images.

4. Discussion

4.1. Experimental Validation of the Anode Heel Effect

The experimental results confirmed the presence of significant dose distribution asymmetry caused by the anode heel effect, with increased intensities on the cathode side and decreased intensities on the anode side. These findings were consistent across all tested tube potentials, validating the physical basis of the effect. These findings highlight the necessity of incorporating the anode heel effect in Monte Carlo simulations to improve both dose calculation accuracy and imaging realism, particularly for clinical dosimetry and research applications.

4.2. Machine Learning Model Performance

The Gradient Boosting Regressor (GBR) successfully captured the complex, non-linear variations in beam intensity associated with the anode heel effect. Compared to simpler regression models, the GBR demonstrated superior accuracy, achieving a high coefficient of determination R^2 and low Mean Squared Error (MSE). This performance highlights the potential of AI-based approaches in enhancing Monte Carlo simulations, particularly for phenomena requiring energy-dependent modeling.

4.3. Integration into Monte Carlo Simulations

The integration of AI-predicted beam weights into the OpenGATE and GGEMS frameworks enabled accurate replication of the anode heel effect. Fluence and dose map comparisons confirmed that the AI-enhanced simulations closely mirrored experimental measurements. This approach bridges the gap between experimental data and simulation accuracy, providing a robust tool for applications such as dose optimization and radiation safety.

4.4. Clinical and Research Implications

In clinical settings, accurately modeling the anode heel effect enhances dosimetry precision, which is critical for procedures that require controlled radiation exposure. The AI-driven approach also supports research by streamlining the simulation of realistic X-ray beam characteristics. Future work will focus on incorporating additional beam parameters, such as filtration and off-axis intensity profiles, to enhance the realism and applicability of the model in diverse X-ray imaging scenarios.

5. Conclusion

This study presents an innovative method for modeling the anode heel effect by integrating experimental data, machine learning, and Monte Carlo simulations. The results demonstrate that AI-driven modeling provides a scalable and accurate solution for predicting X-ray beam intensity distributions across varying tube potentials. The integration of the Gradient Boosting Regressor into OpenGATE and GGEMS frameworks significantly improved the realism of simulated dose distributions, bridging the gap between experimental and simulation-based studies.

Future research will aim to extend the model by integrating additional beam characteristics, such as dynamic variations during fluoroscopy, and validating its performance across different X-ray systems and clinical imaging protocols. By advancing the accuracy of dosimetric simulations, this approach contributes to improved radiation measurements and optimized imaging protocols in both clinical and research domains.

6. Acknowledgements

We acknowledge the support of the French Brittany Region, PLaTIMeD and MoCaMed.

Usage Note

The modeled X-ray source described in this article is freely available for use in research and simulation studies. It is compatible with tools such as OpenGATE and can be accessed through this implementation for the Siemens Cios Alpha X-ray system. We kindly request that users cite this article as a reference when utilizing the model in their work. Proper citation ensures acknowledgment of the development efforts and supports the dissemination of this resource within the scientific community.

- [1] Panagiotis Papadimitroulas. Dosimetry applications in gate monte carlo toolkit. *Physica Medica*, 41:136–140, 2017.
- [2] David Sarrut et al. The opengate ecosystem for monte carlo simulation in medical physics. *Physics in Medicine and Biology*, 67(18):18, 2022.
- [3] J Anthony Seibert. X-ray imaging physics for nuclear medicine technologists. part 1: Basic principles of x-ray production. *Journal of nuclear medicine technology*, 32(3):139–147, 2004.
- [4] David Sarrut, Nils Krahl, and Jean-Michel Létang. Generative adversarial networks (gan) for compact beam source modelling in monte carlo simulations. *Physics in Medicine & Biology*, 64(21):215004, 2019.
- [5] Seong-gyu Shin and Hyo-Yeong Lee. The anode heel effect caused by changing the angle of x-ray tube. *Journal of the Korean Society of Radiology*, 10(6):435–442, 2016.
- [6] Rolf Behling and Florian Grüner. Diagnostic x-ray sources—present and future. *Nuclear Instruments and Methods in Physics Research Section A: Accelerators, Spectrometers, Detectors and Associated Equipment*, 878:50–57, 2018.
- [7] Richard Francis Mould. The early history of x-ray diagnosis with emphasis on the contributions of physics 1895-1915. *Physics in Medicine & Biology*, 40(11):1741, 1995.
- [8] Sangeetha Prabhu, Divya Kumari Naveen, Sandhya Bangera, and B Subrahmanya Bhat. Production of x-rays using x-ray tube. In *Journal of Physics: Conference Series*, volume 1712, page 012036. IOP Publishing, 2020.
- [9] G. Poludniowski, A. Omar, R. Bujila, and P. Andreo. Technical note: Spekpy v2.0—a software toolkit for modeling x-ray tube spectra. *Medical Physics*, 2021.
- [10] Bahaa Nasr, Mateo Villa, Didier Benoit, Dimitris Visvikis, and Julien Bert. Monte carlo dosimetry validation for x-ray guided endovascular procedures. *Annals of Vascular Surgery*, 99:186–192, 2024.
- [11] Julien Bert, Hector Perez-Ponce, Ziad El Bitar, Sébastien Jan, Yannick Boursier, Damien Vintache, Alain Bonissent, Christian Morel, David Brasse, and Dimitris Visvikis. Geant4-based Monte Carlo simulations on GPU for medical applications. *Phys. Med. Biol.*, 58(16):5593–5611, 2013.
- [12] Rolf Behling. X-ray sources: 125 years of developments of this intriguing technology. *Physica Medica*, 79:162–187, 2020.
- [13] Frank E Zink. X-ray tubes. *Radiographics*, 17(5):1259–1268, 1997.
- [14] John M. Boone and J. Anthony Seibert. An accurate method for computer-generating tungsten anode x-ray spectra from 30 to 140 kV. *Medical Physics*, 24(11):1661–1670, 1997.
- [15] Artur Omar, Pedro Andreo, and Gavin Poludniowski. A model for the emission of k and l x rays from an x-ray tube. *Nuclear Instruments and Methods in Physics Research Section B: Beam Interactions with Materials and Atoms*, 437:36–47, 2018.
- [16] Michael K Fix, Paul J Keall, Kathryn Dawson, and Jeffrey V Siebers. Monte carlo source model for photon beam radiotherapy: photon source characteristics: Monte carlo source model. *Medical physics*, 31(11):3106–3121, 2004.
- [17] Siemens Healthcare GmbH. Cios Alpha. <https://www.siemens-healthineers.com/surgical-c-arms-and-navigation/mobile-c-arms/cios-alpha-cmos>, 2020. [Online]. Available: <https://www.siemens-healthineers.com/surgical-c-arms-and-navigation/mobile-c-arms/cios-alpha-cmos>.
- [18] PTW Dosimetry. NOMEX Multimeter, 2024. [Online; accessed 27-July-2024].
- [19] Weixin Yao and Longhai Li. A new regression model: modal linear regression. *Scandinavian Journal of Statistics*, 41(3):656–671, 2014.
- [20] Mariette Awad, Rahul Khanna, Mariette Awad, and Rahul Khanna. Support vector regression. *Efficient learning machines: Theories, concepts, and applications for engineers and system designers*, pages 67–80, 2015.
- [21] Alexey Natekin and Alois Knoll. Gradient boosting machines, a tutorial. *Frontiers in neurorobotics*, 7:21, 2013.
- [22] Seon-Chil Kim and Hong-Moon Jung. A study on performance of low-dose medical radiation shielding fiber (rsf) in ct scans. *International Journal of Technology*, 4(2), 2013.